J Herbmed Pharmacol. 2026; 15(1): 122-134.

http://www.herbmedpharmacol.com doi: 10.34172/jhp.2026.53027

Journal of Herbmed Pharmacology

A promising computational study of ovarian cancer treatment of the isolated compound 5,7-dihydroxy-3(*R*)-methylphthalide

Agus Dwi Ananto[1*], Tendy Oktriawan[2*], Kasta Gurning[2,3], Muhammad Idham Darussalam Mardjan[2], Tri Joko Raharjo[2], Yoshihito Shiono[4], Winarto Haryadi[1*]

[1]Departement of Pharmacy, Faculty of Medicine and Health Sciences, University of Mataram, Indonesia
[2]Department of Chemistry, Faculty of Mathematics and Natural Sciences, Universitas Gadjah Mada, Yogyakarta, Indonesia
[3]Department of Pharmacy, Universitas Senior Medan, Medan, Indonesia
[4]Department of Food, Life, and Environmental Sciences, Faculty of Agriculture, Yamagata University, Tsuruoka, Yamagata, Japan

ARTICLE INFO

Article Type:
Short Communication

Article History:
Received: 19 Mar. 2025
Revised: 19 Oct. 2025
Accepted: 20 Oct. 2025
epublished: 1 Jan. 2026

Keywords:
ADMET
Bioinformatics
Molecular docking
Molecular dynamics
Ovarian cancer

ABSTRACT

Introduction: Ovarian cancer is a serious disease with high incidence and mortality in women, despite advances in surgical and medical therapies. Continuous efforts to develop safer and more effective treatments are crucial. The aim of this study was to explore the potential of 5,7-dihydroxy-3(*R*)-methylphthalide against ovarian cancer.

Methods: This study utilized a bioinformatics approach with network pharmacology to collect active compounds and genes related to ovarian cancer, predict targets, perform network analysis, gene and pathway enrichment, molecular docking and molecular dynamics, and ADMET (Absorption, Distribution, Metabolism, Excretion, and Toxicity) prediction.

Results: The bioinformatics approach revealed that the SRC protein was the most promising target among 28 potential target genes related to ovarian cancer influenced by the active compound. Molecular docking results indicated that the compound formed major hydrogen bond interactions with amino acid residues and exhibited relatively low binding energy values, indicating strong binding affinity. Molecular dynamics simulations confirmed the stability of the protein and ligand over 100 ns. MM-PBSA (Poisson-Boltzmann Surface Area Molecular Mechanics) analysis indicated lower binding energy for the compound. ADMET analysis indicated that the evaluated compounds did not violate the Lipinski, Ghose, Veber, and Egan rules, considering that the formulation changes showed no indication of cytotoxicity, mutagenicity, hepatotoxicity, neurotoxicity, cardiotoxicity, or immunotoxicity.

Conclusion: The compound 5,7-dihydroxy-3(*R*)-methylphthalide has potential compared to its native ligand (1BU) and epirubicin as a control drug in targeting the SRC protein in ovarian cancer. Further in vitro and in vivo evaluation is needed to validate the activity.

Implication for health policy/practice/research/medical education:
The computational study of 5,7-dihydroxy-3(*R*)-methylphthalide reveals its potential as a natural ovarian anticancer agent, warranting further experimental validation and clinical research.

Please cite this paper as: Ananto AD, Oktriawan T, Gurning K, Mardjan MID, Raharjo TJ, Shiono Y, et al. A promising computational study of ovarian cancer treatment of the isolated compound 5,7-dihydroxy-3(*R*)-methylphthalide. J Herbmed Pharmacol. 2026;15(1):122-134. doi: 10.34172/jhp.2026.53027.

Introduction

Ovarian cancer is the fourth leading cause of cancer-related deaths among women, with over 300,000 new cases diagnosed globally each year and more than 20,000 fatalities attributed to the disease (1,2). It primarily affects women who are middle-aged and older (3). The incidence is especially high among postmenopausal women, and the total number of new diagnoses is anticipated to rise in parallel with the growing proportion of the elderly population (4). Ovarian cancer is generally categorized into three primary types based on the origin of the tumor cells: epithelial tumors, germ cell tumors, and sex cord-stromal tumors (5-7). Epithelial ovarian cancer constitutes the predominant subtype, accounting for approximately

***Corresponding authors**: Agus Dwi Ananto, Email: agus_da@unram.ac.id; Tendy Oktriawan, Email: tendy.oktriawan@mail.ugm.ac.id; Winarto Haryadi, Email: wnrt_haryadi@ugm.ac.id

85%-90% of all ovarian cancer cases (8). These tumors are developed from the surface epithelial cells that cover the ovary and encompass various histological subtypes, including high-grade serous carcinoma, low-grade serous carcinoma, mucinous carcinoma, endometrioid carcinoma, and clear cell carcinoma (9,10). Among these, high-grade serous carcinoma is the most common and aggressive subtype, frequently diagnosed at an advanced stage due to its rapid progression (11). Despite available treatments, the survival rate for ovarian cancer patients remains low, with only about 30% of patients surviving (12,13). Therefore, effective treatment strategies for this cancer are critical to improving survival and saving lives in the future.

Several ovarian cancer treatments are available today, such as surgery and chemotherapy (14). Surgical removal of affected ovaries is the ultimate treatment option, but this practice often affects other reproductive organs that can have consequences on reproductive fertility and other complications (15,16). Therefore, chemotherapy is the most preferable. Chemotherapy often requires selective and non-toxic chemicals that can inhibit cancerous cells and evade normal cells, but available approved choices are not effective (17,18).

Epirubicin is a standard drug for ovarian cancer, but it has been found to cause blood in the urine or stools (19), bleeding gums (20), cough (21), swollen lymph nodes (22), menorrhagia (23), sore mouth (24), ulcer (25), chest pain (26), skin changes (27), nausea (28), fatigue (29), diarrhoea (30), and hair loss (31). These negative impacts increase the difficulty for cancer patients to recover. In contrast, anticancer drugs from natural resources have been considered safe and non-toxic treatments (32). Some natural products have been isolated and investigated as anticancer agents for ovarian cancer cells (33). Many natural compounds have demonstrated good SI (Selectivity Indices) greater than 1.5, indicating strong activity against ovarian cancer cell lines while sparing normal cells (34), as shown in Table 1.

In-silico studies play a crucial role in the discovery and development of new drugs for ovarian cancer by significantly accelerating the research process while reducing costs and resource consumption (38). The bioinformatics approach enables researchers to analyze vast biological data and identify potential molecular targets specific to ovarian cancer. Molecular docking further aids in predicting the binding affinity and interaction mode between candidate compounds and target proteins (39). Complementing this, molecular dynamics simulations provide deeper insight into the stability and behavior of drug-target complexes over time (40). Additionally, ADMET (Absorption, Distribution, Metabolism, Excretion, and Toxicity) analysis is vital to evaluate the pharmacokinetic and safety profiles of new compounds early in the drug development pipeline, minimizing the risk of late-stage failures (41). Together, these in-silico techniques form an integrated framework that enhances the efficiency and precision of discovering novel ovarian cancer drugs, ultimately facilitating the translation of promising compounds from the laboratory to clinical use. Many studies have explored that the in-silico approach correlates positively with in vitro testing results, as demonstrated in Table 2. However, the application of an in-silico approach specifically targeting polyketide-derived compounds for ovarian cancer treatment remains limited, indicating an area with potential for further research and development.

Building on this research, our previous work isolated

Table 1. Selectivity index (SI) of natural products against ovarian cancer cells

Compound	IC_{50} (μM)		SI	Category	Ref.
	Ovarian cancer cells	Normal cells			
Monoterpene derivative	A2780: 0.77	NIH/3T3: 4.36	5.66	Not cytotoxic	(35)
Evernic acid	OVCAR-3: 10	OSE: 159	15.90	Not cytotoxic	(36)
Corilagin	A2780: 47	IOSE-80: 263	5.59	Not cytotoxic	(37)

OSE: Ovarian surface epithelium; IOSE-80: Immortalized ovarian surface epithelium 80.

Table 2. In-silico studies of drug compound development

Protein by bioinformatics approach	Compound	Key amino acid in hydrogen bond interaction	Binding affinity (kcal/mol)	RMSD of MD simulation (Å)	Bioactivity	Ref.
lrp proteins	Xanthyl chlorocinnamate	Val59 and Gly60	-6.00	-	MIC: *S. aureus*: 6.25 ppm *E. coli*: 12.5 ppm	(42)
JAK2 protein	Petunidin	Lys581, Gln626, Val629, Lys630, and Ser698	-9.46	<3	SARS-Cov-2: nd	(43)
CXCL2 protein	Quercetin	Asn73, Lys21	-7.20	<6	Psosiaris: nd	(44)
CXCR4 protein	Triptolide	His87	-10.10	<10		

RMSD: Root mean square deviation; MD: molecular dynamics; MIC: Minimum inhibitory concentration.

natural compounds from an endophytic fungus named *Xylaria brevipes* (45). This fungus was macerated with methanol and then partitioned further using an ethyl acetate solvent. The chromatographic process resulted in the separation of 12 fractions, one of which included a novel compound identified as 5,7-dihydroxy-3(*R*)-methylphthalide, as shown in Figure 1a. This compound exhibited a low cytotoxicity profile with a good mortality rate at a shallow concentration. To explore the potential applications of this compound, we utilized a bioinformatics approach, molecular docking, molecular dynamics simulations analysis, and ADMET analysis, with a focus on its ability to target ovarian cancer cells.

Materials and Methods

Materials

The 3D single-crystal structure of SRC protein (PDB: 3F3V) was obtained from the RCSB Protein Data Bank website. Computational analyses were performed using a PC equipped with an Intel® Xeon processor CPU E5-2650 v2 @2.60 GHz. The software utilized included GaussView 5.0, Gaussian 09W, Chimera 1.13.1, AutoDock 4.2, Discovery Studio 2019, and YASARA. Additionally, several databases such as SwissTargetPrediction, Cytoscape 3.10.1, Online Mendelian Inheritance in Man (OMIM), DisGeNET, Therapeutic Targets Database (TTD), and GeneCards were employed to investigate potential biological targets and their associations.

Isolated active compound

The active compound, 5,7-dihydroxy-3(*R*)-methylphthalide, was isolated from the ethyl acetate extract of the fungus *X. brevipes* in previous studies. This extract was derived through sequential partitioning of the methanol extract using n-hexane, chloroform, and ethyl acetate, as described in previous studies (45). The structures of the isolated compounds were constructed using GaussView 5.0 software and optimized with Gaussian 09W. The optimization process employed density functional theory at the B3LYP/6-311G+(d,p) level of theory (46,47).

Identification of the potential activity of the active compound against ovarian cancer

For specific targets of active compounds, Simplified Molecular Input Line Entry System (SMILES) data were obtained using ChemDraw software and then uploaded to the SwissTargetPrediction database, with the species parameter set to Homo sapiens. The resulting target prediction data was downloaded in CSV format and processed using Microsoft Excel for further data cleaning and organization.

Simultaneously, ovarian cancer-specific targets were collected from the GeneCards database by searching for the keyword "ovarian cancer". The gene symbols obtained from the GeneCards dataset and the predicted protein-coding targets from SwissTargetPrediction were then input ino VENNY 2.1 to identify overlapping proteins.

The intersection of these datasets represents potential target proteins implicated in ovarian cancer that are also predicted to interact with the active compound, providing insight into the compound's possible therapeutic effects (48-50).

Protein-protein interaction (PPI) analysis and screening

PPI represents the relationships between two or more proteins, influenced by biochemical properties, hydrophobicity, and electrostatic interactions. Proteins are essential participants in numerous biological processes in both normal and pathological states. PPI networks visualize the interconnections between genes and proteins, serving as a critical area of bioinformatics research (51-53). In this study, proteins shared between the active compound and ovarian cancer were uploaded to the STRING database with parameters set for *Homo sapiens* and a confidence threshold of 0.4, while other settings remained default. The resulting PPI data, including node1, node2, and the combined score, were exported and imported into Cytoscape 3.10.1 to construct an interaction network. To identify key proteins, a top target analysis was performed using the CytoHubba plugin in Cytoscape, highlighting the top 10 proteins based on three centrality measures: betweenness centrality, indegree centrality, and closeness centrality. Betweenness centrality evaluates node importance based on connections with immediate neighbors, indegree centrality measures the number of direct links a protein has, and closeness centrality assesses the average shortest distance to all other nodes, reflecting network influence. This combined approach provides a robust identification of hub proteins (54,55).

Gene ontology (GO) and Kyoto Encyclopedia of Genes and Genomes (KEGG) pathway analysis

GO and KEGG analyses were carried out focusing on biological processes, cellular components, gene function, and molecular functions using ShinyGO 0.77. Bioinformatic analysis of STRING data was performed by mapping the target proteins of active compounds associated with ovarian cancer, revealing the molecular mechanisms through which these compounds act in ovarian cancer treatment (56).

Molecular docking analysis

To validate the docking protocol, redocking was performed using the native ligand 1BU of the SRC protein (PDB: 3F3V). Docking simulations were carried out with AutoDock4, applying a grid box sized 40 × 40 × 40 Å centered at coordinates (-4.504, 34.198, -7.299). Lamarckian genetic algorithm was used with 100 runs to explore the binding conformations and predict the

most favorable ligand-protein interactions. Following the same parameters used in the redocking process, the active compound was docked into the receptor binding sites to evaluate their interactions and binding affinities (57).

Molecular dynamics simulation

Molecular dynamics simulations of the complex were conducted using YASARA software and the md_runmembrane.mcr script. The simulation was set to a temperature of 310 K, pressure of 1 atm (NPT ensemble), pH 7.4, and a NaCl concentration of 0.9% to replicate physiological conditions. Energy minimization was performed using the steepest descent method followed by simulated annealing minimization to achieve a density of 0.999 g/mL. An initial equilibration phase of 250 ps was carried out to stabilize the system before running production simulations for 100 ns with a timestep of 2.5 fs, recording snapshots every 100 ps. After the simulation, analyses were performed using md_analyze.mcr macro in YASARA to calculate root mean square deviation (RMSD), radius of gyration (RoG), root mean square fluctuation (RMSF), and solvent accessible surface area (SASA), and dictionary of secondary structure of proteins (DSSP) values. Additionally, the BEcalculation.mcr macro was employed to assess the MM-PBSA binding energy (58,59).

Secondary structure analysis

The validation of the 3D protein model was carried out through secondary structure analysis using a Ramachandran (RAM) plot, which evaluates the dihedral angles phi (φ) and psi (ψ) of amino acid residues. The RAM plot for the protein was generated using the PDB-Sum online tool (60).

ADMET study

Drug-likeness was evaluated based on Lipinski's rule of five, along with additional criteria outlined by the Ghose, Veber, and Egan rules. Molecular properties, including molecular weight, the number of heavy atoms, hydrogen bond acceptors, hydrogen bond donors, rotatable bonds, molar refractivity, topological polar surface area, and log P, were predicted using SwissADME. Furthermore, a comprehensive ADMET analysis was performed using the pkCSM software to assess the pharmacokinetic and safety profiles of the compound (61).

Results

Identification of active compound and ovarian cancer target protein using a bioinformatic approach

The compound-specific targets of the active compound 5,7-dihydroxy-3(*R*)-methylphthalide were identified using Swiss Target Prediction, which yielded 30 top target genes. Concurrently, ovarian cancer-specific target genes were retrieved from the GeneCards database, resulting

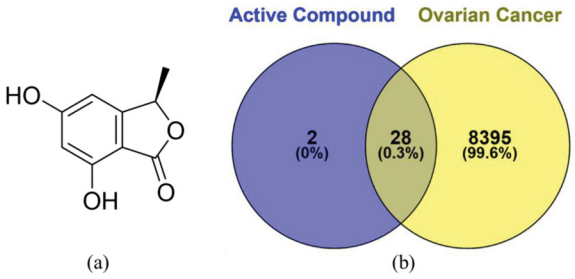

Figure 1. (a) The chemical structure of 5,7-dihydroxy-3(*R*)-methylphthalide and (b) The intersection of proteins associated with the active compound and proteins linked to ovarian cancer targets.

in a list of 8,423 related genes. The intersection of active compounds and ovarian cancer genes was performed using a Venn diagram, and 28 potential target genes related to ovarian cancer affected by the active compound were obtained (Figure 1b). These 28 target genes were then built and analyzed in the STRING database to obtain a PPI network, setting Homo sapiens as the organism and a confidence threshold of 0.40 (Figure 2a). The target-active compound intersection was then imported into Cytoscape 3.10.0 to create a map of the potential main target protein interaction network (Figure 2b). Notably, the top 10 protein targets were identified as SRC, CCNA2, PARP1, CCNA1, KDR, CDK2, MET, PTK2, CCNT1, and CA9 based on minimum neighborhood connectivity (MNC) (Figure 2c), Degree Centrality (Figure 2d), and Closeness Centrality (Figure 2e).

GO and KEGG pathway analyses were performed using the bioinformatics tool ShinyGO 0.77 to investigate the mechanisms of 28 target proteins involved in ovarian cancer treatment. The GO analyses, such as biological processes, cellular components, and molecular functions, are shown respectively in Figure 3a-3c. In addition, KEGG pathways corresponding to potential targets of these active compounds are shown in Figure 3d.

Molecular docking of 5,7-dihydroxy-3(*R*)-methylphthalide against SRC protein

The docking parameters for the active compounds were validated through redocking of 1BU, the native ligand. The redocking process yielded an RMSD value of 0.74 Å, confirming that the docking parameters were reliable and acceptable. The superimposed conformations of 1BU before and after redocking showed minimal structural differences (Figure 4a-4d).

Molecular dynamics simulations of 5,7-dihydroxy-3(*R*)-methylphthalide against SRC protein

The RMSD and RMSF values were measured for the active compound, epirubicin, and native ligand 1BU (Figure 5a-5b). The RMSD values for the active compound, epirubicin, and 1BU were 3.371 ± 0.270

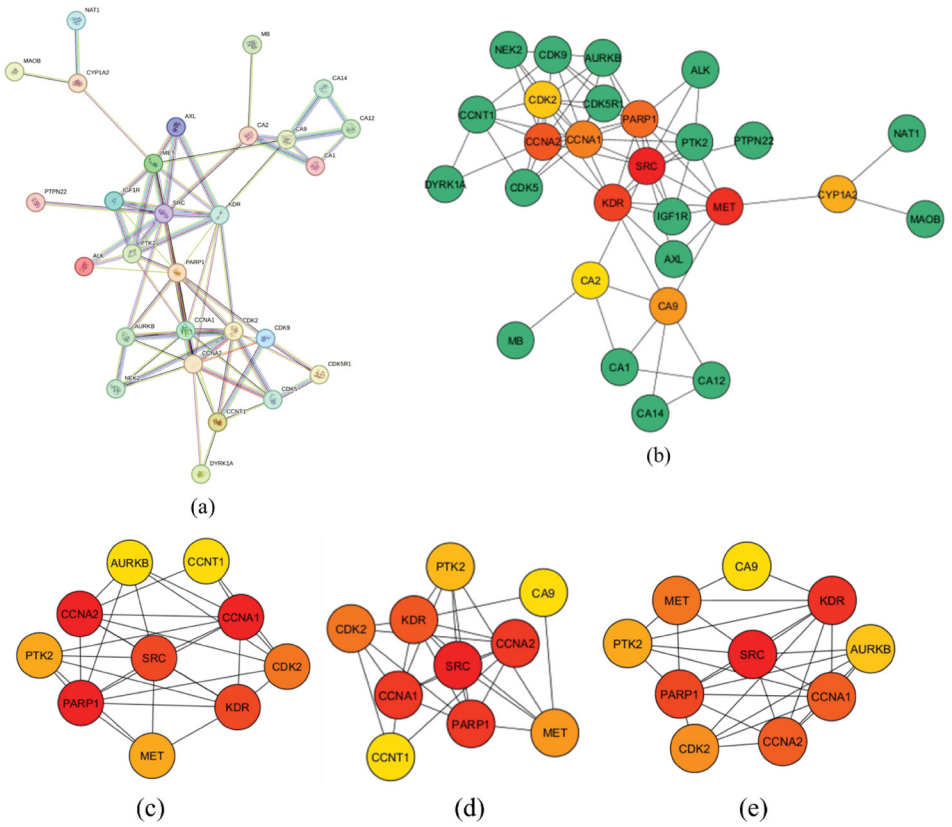

Figure 2. Analysis of protein-protein interaction (PPI). (a) PPI network built from the intersection of Venn diagrams using STRING analysis; (b) PPI network visualized with Cytoscape; (c) Protein target network ranked by minimum neighborhood connectivity; (d) Degree centrality; (e) Closeness centrality.

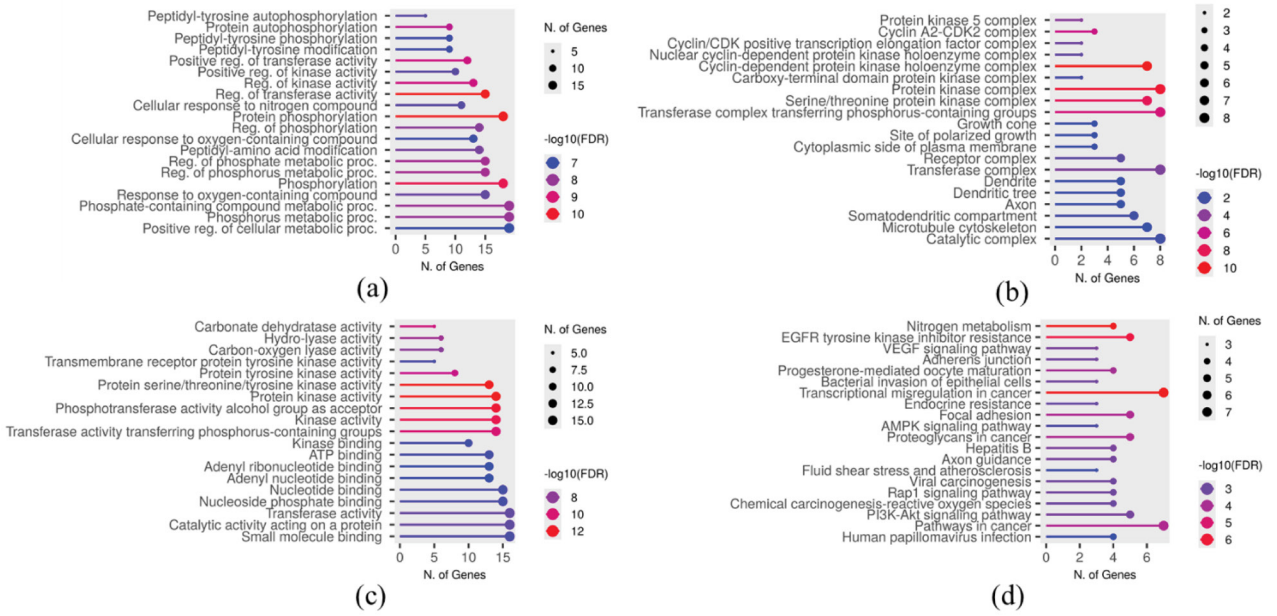

Figure 3. The analysis of gene ontology (GO) categories. (a) Biological processes; (b) Cellular components; (c) Molecular functions; (d) Kyoto encyclopedia of genes and genomes (KEGG) pathways enrichment, based on the potential targets of active compounds in the ovarian cancer treatment.

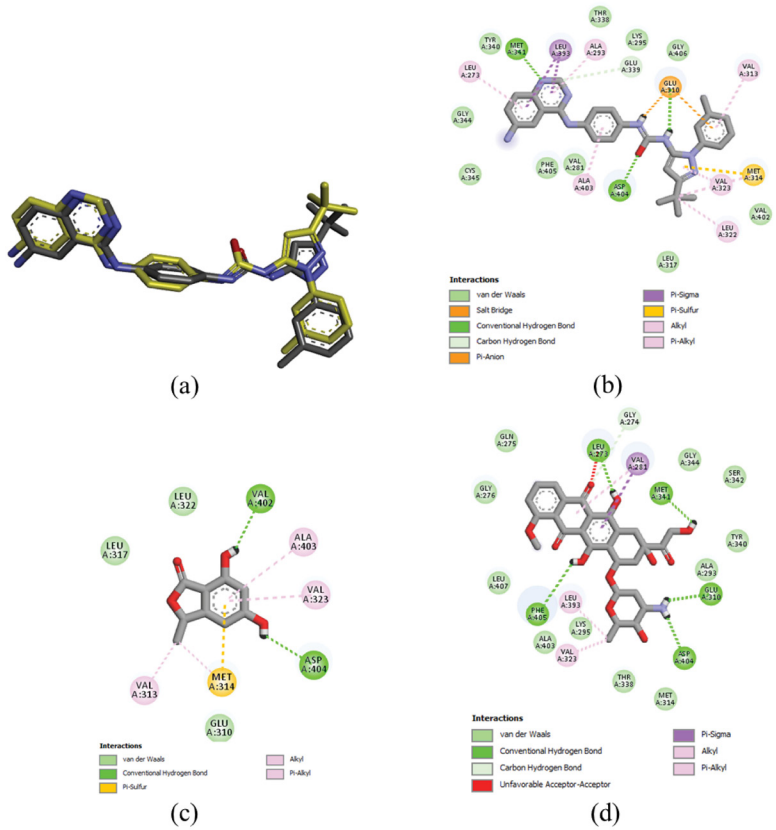

Figure 4. The superimposed conformations of 1BU before and after redocking. (a) The superimposed structure of 1BU as the native ligand before (black) and after (yellow) redocking process; (b) The visualization of chemical interactions of 1BU; (c) 5,7-dihydroxy-3(*R*)-methylphthalide; (d) Epirubicin with the active site of SRC protein.

Å, 4.085 ± 0.304 Å, and 3.492 ± 0.238 Å, respectively. Furthermore, the RMSF values were 1.82 ± 0.756 Å for the active compound, 1.59 ± 0.631 Å for epirubicin, and 1.77 ± 0.676 Å for 1BU.

The SRC protein complexed with the active compound generated the most favored regions with 211 residues (85.6%), allowed regions with 34 residues (13.8%), and generously allowed regions with 2 residues (0.8%). Meanwhile, the SRC protein complexed with epirubicin generated the most favored areas with 210 residues (85.0%), allowed regions with 34 residues (13.8%), and generously allowed regions with 2 residues (0.8%). Additionally, the SRC protein complex with native ligand generated the most favored regions with 208 residues (84.2%), allowed regions with 35 residues (14.2%), and generously allowed regions with 3 residues (1.2%). The DSSP analysis demonstrated that the secondary structural elements of the SRC protein, including helices, sheets, turns, coils, helix-310, and helix-Pi fractions, remained stable throughout the 100 ns molecular dynamics simulations (Figure 6a-6c).

RoG values were 2.07 ± 0.016 nm for the active compound, 2.04 ± 0.017 nm for epirubicin, and 2.03 ± 0.013 nm for the native ligand (1BU). In addition, SASA values were 147.76 ± 2.72 nm^2 for the active compound, 151.26 ± 3.41 nm^2 for the epirubicin, and 150.38 ± 2.77 nm^2 for the 1BU. These results are displayed in Figure 5c and 5d. Molecular mechanics Poisson-Boltzmann surface area (MM-PBSA) calculations indicated binding energies of -4.12 kJ/mol for the active compound, -175.79 kJ/mol for epirubicin, and 29.16 kJ/mol for 1BU, as summarized in Table 3.

ADMET study

Comprehensive ADMET analysis of the active compound, epirubicin, and 1BU is presented in Table 4, covering drug-likeness, absorption, distribution, metabolism, excretion, and toxicity. This comprehensive evaluation provides insights into the pharmacokinetic and safety profiles of each compound, which are crucial for assessing their potential as effective and safe therapeutic agents.

Discussion

The bioinformatics approach is crucial in investigating natural product compounds for ovarian cancer treatment. It enables comprehensive analysis of molecular interactions, target identification, and pathway elucidation, thereby accelerating drug discovery and development. By integrating computational tools, researchers can efficiently screen, predict, and optimize

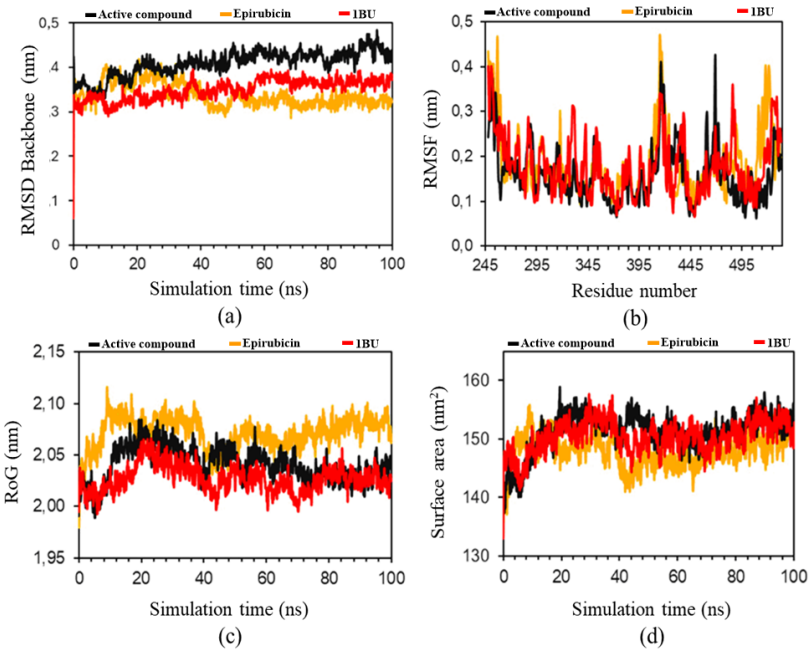

Figure 5. Backbone root mean square deviation (RMSD; a), root mean square fluctuation (RMSF; b), RoG (radius of gyration; c), and solvent accessible surface area (SASA; d) analysis during 100 ns simulation of SRC protein.

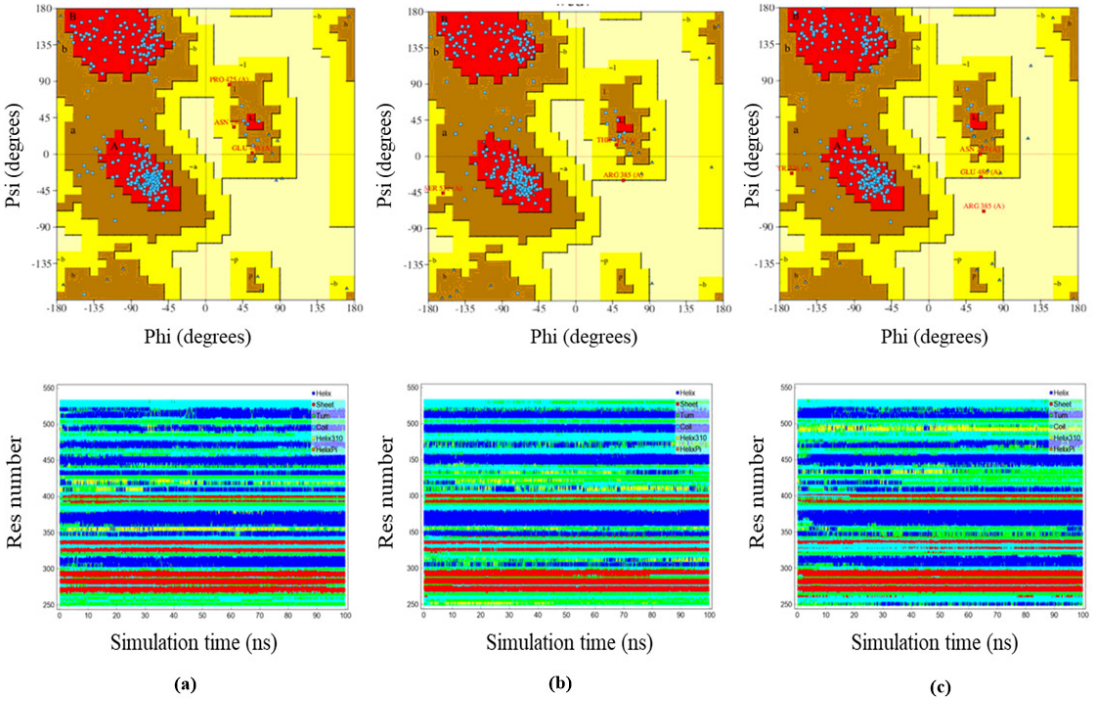

Figure 6. Ramachandran plot (RAM) and dictionary of secondary structure of proteins (DSSP) analysis of SRC protein: (a) 5,7-dihydroxy-3(R)-methylphthalide, (b) epirubicin, and (c) native ligand (1BU).

the therapeutic efficacy and safety of natural compounds, ultimately contributing to more effective and targeted cancer therapies. In this study, SRC protein was identified as the most significant protein among 28 proteins related to ovarian cancer based on MNC, Degree centrality, and Closeness centrality measures from the PPI network, which were further supported by GO and KEGG pathway analyses.

SRC protein is a non-receptor tyrosine kinase that plays a central role in various cellular signaling pathways related to cancer development and progression. Its role in coordinating metabolic pathways further supports cancer

Table 3. Molecular mechanics Poisson-Boltzmann surface area (MM-PBSA) calculation for various compounds after molecular dynamics simulations in the active site of SRC protein

Energy	Energy value (kcal/mol)		
	Active compound	Epirubicin	1BU
EpotRecept	-9864.74 ± 801.84	-9330.45 ± 858.03	-9397.20 ± 935.18
EsolvRecept	-23652.99 ± 948.26	-23825.15 ± 965.30	-24660.64 ± 1435.75
EpotLigand	-176.62 ± 17.51	523.75 ± 28.78	-710.16 ± 26.50
EsolvLigand	-162.08 ± 18.88	-497.44 ± 23.62	-218.72 ± 14.30
EpotComplex	-10174.63 ± 806.27	-9110.54 ± 879.98	-10508.28 ± 943.53
EsolvComplex	-23639.04 ± 953.48	-23842.97 ± 983.36	-24507.05 ± 1445.54
Binding energy	-43.12 ± 34.97	-175.79 ± 38.77	29.16 ± 33.13

Table 4. Absorption, distribution, metabolism, excretion, and toxicity (ADMET) results of the active compound

Pharmacokinetic parameter	Native ligand (1BU)	Epirubicin	Active compounds
Drug-likeness			
Molecular weight (g/mol)	506.61	543.52	180.16
Log P	7.19	0.70	1.33
H-bond donor	4	6	2
H-bond acceptor	8	12	4
Topological polar surface area (Å^2)	122.78	206.07	66.76
Rotatable bonds	8	5	0
Absorption			
Water solubility (log mol/L)	-3.30	-2.91	-1.81
HIA (%)	92.23	62.37	93.32
Caco-2 permeability (cm/s)	-0.13	0.46	1.08
Distribution			
log BBB permeability	-1.04	-1.38	-0.35
VDss for human	-1.01	1.65	-0.13
CNS permeability	-1.54	-4.31	-3.29
Metabolism			
CYP2D6 inhibitor	Inactive	Inactive	Inactive
CYP2E1 inhibitor	Inactive	Inactive	Inactive
CYP3A4 inhibitor	Inactive	Inactive	Inactive
CYP2C9 inhibitor	Inactive	Inactive	Inactive
CYP2C19 inhibitor	Inactive	Inactive	Inactive
CYP1A2 inhibitor	Inactive	Inactive	Inactive
Excretion			
Total clearance (log mL/min/kg)	-0.17	0.99	0.59
Renal OCT2 substrate	No	No	No
Toxicity			
Cytotoxicity	Inactive	Active	Inactive
Mutagenicity	Inactive	Active	Inactive
Hepatotoxicity	Active	Inactive	Inactive
Neurotoxicity	Active	Active	Inactive
Cardiotoxicity	Inactive	Active	Inactive
Immunotoxicity	Inactive	Active	Inactive
hERG I inhibitor	No	No	No
hERG II inhibitor	Yes	Yes	No

cell adaptation and survival in challenging environments. In ovarian cancer, elevated SRC levels are associated with chemoresistance and poor prognosis (62). By interacting with nuclear receptors such as the estrogen receptor, SRC enhances target gene transcription, thereby promoting cancer cell proliferation (63). Additionally, SRC plays a critical role in metastasis by regulating ovarian cancer cell migration and invasion; its downregulation has been shown to significantly reduce these processes (64). Due to its widespread involvement in tumor progression, SRC

is considered a promising therapeutic target, with efforts ongoing to develop inhibitors that can effectively disrupt its signaling and improve cancer treatment efficacy.

Based on KEGG pathway analysis, the SRC protein was significantly associated with EGFR tyrosine kinase inhibitor resistance. Inhibition of SRC played a critical role in regulating key cellular processes such as proliferation, survival, growth, differentiation, motility, and angiogenesis. Additionally, SRC was linked to HER-2 mutations as well as the overexpression of HER-2 and HER-3 within the EGFR signalling pathway, all of which were closely related to targeted inhibition strategies in ovarian cancer. Members of the HER family were frequently overexpressed or dysregulated in ovarian tumors. Moreover, SRC was responsible for the abnormal dimerization of STAT3. Abnormal activation and dimerization of STAT3 contributed to sustained signalling that supports cancer progression, including ovarian cancer, by regulating genes involved in cell growth and metastasis. This interaction between SRC and STAT3 highlighted a critical pathway that could be targeted for therapeutic intervention in tumor progression and drug resistance.

The molecular docking analysis revealed detailed interactions between the SRC protein and three ligands: 1BU as the native ligand, 5,7-dihydroxy-3(*R*)-methylphthalide as the active compound, and epirubicin as a drug for ovarian cancer treatment. 1BU exhibited strong binding affinity toward SRC with a binding energy of -40.50 kJ/mol and a highly favorable binding constant of 0.01 μM. Its interaction profile included multiple hydrogen bonds with key active site residues Met341 (2.30 Å), Asp404 (2.13 Å), and Glu310 (2.00 Å). Additionally, a carbon-hydrogen bond with Glu339, a salt bridge, and a pi-anion interaction with Glu310, as well as a pi-sulfur bond with Met314, contributed to binding stability. The hydrophobic contacts involved Leu273, Leu393, Ala313, Met314, Val323, Leu322, and Ala403, demonstrating a comprehensive engagement with the active site.

The active compound showed a different interaction pattern, with a binding energy of -22.97 kJ/mol and a binding constant of 95.03 μM, indicating a weaker affinity relative to the native ligand. This compound formed hydrogen bonds with Asp 404 (2.22 Å) and Val402 (2.14 Å). Notably, Asp404 played a crucial role in SRC inhibition, as it was involved in interaction with both the native ligand and this compound. Additional hydrophobic interactions were detected with Val313, Met314, Val323, and Ala403, plus a pi-sulfur bond with Met314, which supported moderate binding stability.

Epirubicin, with a binding energy of -38.37 kJ/mol and a binding constant of 0.19 μM, bound SRC with high affinity similar to the native ligand. It formed multiple hydrogen bonds within the active site, involving Leu273 (1.71 Å), Met341 (2.28 Å), Glu310 (1.90 Å), Asp404 (2.11 Å), and Phe405 (2.84 Å). However, an unfavorable acceptor-acceptor interaction with Leu273 may reduce overall binding efficiency. A carbon-hydrogen bond with Gly274 and hydrophobic interaction with Val281, Leu393, and Val323 further participated in ligand stabilization.

In summary, 1BU demonstrated the strongest binding affinity to SRC by engaging multiple key residues via diverse interactions, serving as a benchmark for inhibitor binding. Epirubicin showed comparable binding strength, with extensive hydrogen bonding to the same active site residues but with some unfavorable contacts. In contrast, the active compound exhibited moderate binding affinity, maintaining critical interactions with Asp404 but with fewer hydrophobic contacts and weaker overall binding energy. These findings suggest that while the active compound can interact with SRC's active site, optimization may be needed to enhance its binding affinity relative to more potent ligands like 1BU and epirubicin.

RAM analysis identified zero residues in the disallowed regions for the active compound, whereas epirubicin and 1BU each showed one residue, signalling slightly better overall structural integrity for the active compound. This finding aligns with the DSSP secondary structure analysis, which confirmed the SRC protein's secondary structural elements remained stable throughout the simulation for all complexes. RoG values were comparable among all ligands, such as 2.07 ± 0.016 nm for the active compound, 2.04 ± 0.017 nm for epirubicin, and 2.03 ± 0.013 nm for 1BU, indicating similar compactness and folding stability of protein-ligand complexes. SASA values were also close, with 147.76 ± 2.72 nm^2 for the active compound, 151,26 ± 3.41 nm^2 for epirubicin, and 150.38 ± 2.77 nm^2 for 1BU, suggesting no significant difference in solvent exposure upon binding. The binding free energy calculated by MM-PBSA yielded the most favorable value for epirubicin at -175.79 kJ/mol, followed by the active compound at -43.12 kJ/mol, while 1BU exhibited a positive binding energy of 29.16 kJ/mol. Despite the highest binding energy favoring epirubicin, the active compound showed superior structural stability, indicated by its lower RMSD and zero disallowed residues in RAM. In summary, considering both structural stability and binding energetics from the MD simulation data, epirubicin demonstrated the strongest binding affinity energetically, but the active compound exhibited the most stable protein-ligand complex dynamics. The active compound's superior conformational stability suggested that it might be the most promising candidate for further development targeting SRC inhibition under physiological conditions.

ADMET analysis provided a comprehensive evaluation of the pharmacokinetic and safety profiles of three compounds. In terms of drug-likeness, the active compound had the lowest molecular weight (180.16/mol) and a moderate Log P value of 1.33, indicating favorable lipophilicity for drug absorption. It also had the fewest

hydrogen bond donors and acceptors (2 and 4, respectively), which could improve membrane permeability. Compared to 1BU and epirubicin, the active compound had the smallest topological polar surface area (66.76 Å^2), which often correlates with better oral bioavailability. Notably, the active compound had zero rotatable bonds, which may have contributed to a more rigid structure and enhanced binding specificity. Regarding absorption, the active compound displayed the highest water solubility (-1.81 log mol/L) and human intestinal absorption (HIA) at 93.32%, surpassing both 1BU and epirubicin. Its Caco-2 permeability value (1.08 cm/s) was also the highest among the three, suggesting superior intestinal permeability and better absorption potential.

In the distribution phase, the active compound showed better blood-brain barrier (BBB) permeability (-0.35) compared to 1BU and epirubicin, indicating potential central nervous system (CNS) exposure if needed. The VDss was closer to neutral (-0.13) versus positive for epirubicin (1.65) and negative for 1BU (-1.01). Central nervous system penetration predictions showed that the active compound had intermediate CNS permeability (-3.29), better than epirubicin (-4.31), but less than 1BU (-1.54). Metabolically, all three compounds were inactive as inhibitors of major cytochrome P450 enzymes (CYP2D6, CYP2E1, CYP3A4, CYP2C9, CYP2C19, and CYP1A2), reducing the risk of metabolic drug-drug interactions. This was a favorable property for drug candidates regarding safety and metabolic stability. In terms of excretion, total clearance values suggested that epirubicin (0.99) and the active compound (0.59) had higher clearance rates compared to 1BU (-0.17), potentially influencing dosing intervals. Toxicity profiling highlighted clear differences; the active compound was inactive in all tested toxicity categories, including cytotoxicity, mutagenicity, hepatotoxicity, neurotoxicity, cardiotoxicity, and immunotoxicity. In contrast, epirubicin showed multiple toxic effects such as cytotoxicity, mutagenicity, cardiotoxicity, and immunotoxicity. Meanwhile, 1BU exhibited hepatotoxicity and neurotoxicity risks and was a hERG II inhibitor, which raised concerns for cardiac safety. In summary, the active compound demonstrated the most favorable overall ADMET profile. It combined optimal physicochemical properties for drug-likeness and absorption, metabolic stability by not inhibiting CYP enzymes, and a clean toxicity profile without adverse effects. Compared to 1BU and epirubicin, the active compound appeared to be the safest and most promising candidate for further drug development, balancing efficacy potential with reduced safety risks.

Despite the advantages, this study had some limitations. The computational methods, including bioinformatics, molecular docking, and molecular dynamics simulations, could not fully capture the complex biological environment and tumor heterogeneity in vivo. The bioinformatics databases and pathway analyses were limited by the quality and completeness of existing data, which may have introduced bias or overlooked novel targets. Molecular docking and molecular dynamics simulations provided insights into binding stability but did not fully represent cellular pharmacodynamics and pharmacokinetics. The ADMET predictions offered preliminary pharmacokinetic and toxicity profiles but required experimental validation to confirm safety and efficacy. Therefore, further in vitro and in vivo studies are needed to validate the therapeutic potential of the active compound targeting SRC in ovarian cancer.

Conclusion

A comprehensive computational study of 5,7-dihydroxy-3(*R*)-methylphthalide was performed to evaluate whether this compound shows a promising profile for the active compound against ovarian cancer cells. The bioinformatic data revealed that this compound could target 28 proteins related to ovarian cancer disease. Through a PPI network, as well as GO and KEGG pathways, the SRC protein was found to have the most significant protein target for ovarian cancer. The molecular docking study revealed that the active compound had moderate binding affinity, maintaining critical interactions but fewer hydrophobic contacts. Overall, while the active compound interacted with SRC's active site, it needed optimization to improve binding relative to 1BU and epirubicin. Furthermore, molecular dynamics simulations revealed that the active compound's superior stability suggested it was the most promising candidate for further development targeting SRC inhibition under physiological conditions. Moreover, the active compound demonstrated the most favorable ADMET profile, combining good drug-like properties, metabolic stability, and a clean toxicity profile. It appeared to be the safest and most promising candidate for further drug development compared to 1BU and epirubicin. Future studies should focus on structural modifications and experimental validation to confirm its therapeutic efficacy.

Authors' contribution

Conceptualization: Tendy Oktriawan, Muhammad Idham Darussalam Mardjan, Winarto Haryadi.
Data curation: Tendy Oktariawan, Kasta Gurning, Agus Dwi Ananto.
Formal analysis: Tendy Oktariawan, Muhammad Idham Darussalam Mardjan, Kasta Gurning, Agus Dwi Ananto.
Funding acquisition: Muhammad Idham Darussalam Mardjan, Tri Joko Raharjo.
Investigation: Tendy Oktariawan, Kasta Gurning, Agus Dwi Ananto, Muhammad Idham Darussalam Mardjan.
Methodology: Tendy Oktariawan, Tri Joko Raharjo, Yoshihito Shiono, Winarto Haryadi.
Project administration: Tendy Oktariawan, Kasta

Gurning, Agus Dwi Ananto.
Resources: Muhammad Idham Darussalam Mardjan, Tri Joko Raharjo, Yoshihito Shiono, Winarto Haryadi.
Software: Tendy Oktariawan, Agus Dwi Ananto.
Supervision: Tri Joko Raharjo, Yoshihito Shiono, Winarto Haryadi.
Validation: Yoshihito Shiono, Winarto Haryadi.
Visualization: Tendy Oktariawan, Agus Dwi Ananto, Muhammad Idham Darussalam Mardjan.
Writing–original draft: Tendy Oktariawan, Kasta Gurning, Agus Dwi Ananto, Muhammad Idham Darussalam Mardjan.
Writing–review & editing: Tri Joko Raharjo, Yoshihito Shiono, Winarto Haryadi.

Conflict of interests

The authors declared no conflict of interest.

Ethical considerations

The authors have comprehensively evaluated potential issues like plagiarism, data fabrication, and multiple submissions.

Funding/Support

None.

References

1. Ren Y, Xu R, Wang Y, Su L, Su J. Global, regional, and national burden of ovarian cancer in women aged 45 + from 1990 to 2021 and projections for 2050: a systematic analysis based on the 2021 Global Burden of Disease Study. J Cancer Res Clin Oncol. 2025;151(8):225. doi: 10.1007/s00432-025-06277-9.
2. Huhulea EN, Huang L, Eng S, Sumawi B, Huang A, Aifuwa E, et al. Artificial intelligence advancements in oncology: a review of current trends and future directions. Biomedicines. 2025;13(4):951. doi: 10.3390/biomedicines13040951.
3. Tang WZ, Cai QY, Huang KJ, Xu WZ, Li JZ, Pan YR, et al. The global burden of polycystic ovary syndrome, endometriosis, uterine fibroids, cervical cancer, uterine cancer, and ovarian cancer from 1990 to 2021. BMC Public Health. 2025;25(1):1774. doi: 10.1186/s12889-025-22881-3.
4. Mao Y, Gao Y, He Y, Wan Z, Li S, Ding Z, et al. Global burden of cancer in women, 1990-2021: a systematic analysis from the GBD 2021 study. Front Oncol. 2025;15:1633894. doi: 10.3389/fonc.2025.1633894.
5. Laga T, Van Rompuy AS, Busschaert P, Marquina G, Loverix L, Olbrecht S, et al. Single-cell profiling in ovarian germ cell and sex cord-stromal tumours. Br J Cancer. 2025;132(12):1110-23. doi: 10.1038/s41416-025-03012-6.
6. Chowdhury Z, Agrawal S, Gupta S, Rai S, Jethani R, Saha S, et al. The many faces of ovarian sex cord stromal tumors: a clinicopathological analysis at a tertiary cancer center in North India. Surg Exp Pathol. 2025;8(1):13. doi: 10.1186/s42047-025-00184-6.
7. Acosta AM, Colecchia M, Comperat E, Cornejo KM, Gill AJ, Gupta S, et al. Assessment and classification of sex cord-stromal tumours of the testis: recommendations from the testicular sex cord-stromal tumour (TESST) group, an Expert Panel of the Genitourinary Pathology Society (GUPS) and International Society of Urological Pathology (ISUP). Histopathology. 2025;87(5):660-76. doi: 10.1111/his.15482.
8. Smolarz B, Biernacka K, Łukasiewicz H, Samulak D, Piekarska E, Romanowicz H, et al. Ovarian cancer-epidemiology, classification, pathogenesis, treatment, and estrogen receptors' molecular backgrounds. Int J Mol Sci. 2025;26(10):4611. doi: 10.3390/ijms26104611.
9. Alves-Vale C, Galvão B, Silvestre AR, Pereira JS, Bei L, Fernandes JP, et al. Patient-derived organoids as a model to study tubo-ovarian carcinoma: a pathologist's perspective. J Ovarian Res. 2025;18(1):191. doi: 10.1186/s13048-025-01766-4.
10. Kordowitzki P, Lange B, Elias KM, Haigis MC, Mechsner S, Braicu IE, et al. Transforming treatment paradigms: focus on personalized medicine for high-grade serous ovarian cancer. CA Cancer J Clin. 2025;75(5):436-60. doi: 10.3322/caac.70008.
11. Phuong DJ, Pirtz MG, Ralston CQ, Cosgrove BD, Schimenti JC, Flesken-Nikitin A, et al. Aggressive serous carcinomas of the female reproductive tract: cancer-prone cell states and genetic drivers. Cancers (Basel). 2025;17(4):604. doi: 10.3390/cancers17040604.
12. Tian Y, Dong R, Guan Y, Wang Y, Zhao W, Zhang J, et al. UBE2J1 is identified as a novel plasma cell-related gene involved in the prognosis of high-grade serous ovarian cancer. J Transl Med. 2025;23(1):129. doi: 10.1186/s12967-025-06135-9.
13. Gui J. Analysis of global ovarian cancer disease burden and its changing trend from 1990 to 2021. BMC Womens Health. 2025;25(1):352. doi: 10.1186/s12905-025-03904-y.
14. You T, Zhang S. Recent advances in PLGA polymer nanocarriers for ovarian cancer therapy. Front Oncol. 2025;15:1526718. doi: 10.3389/fonc.2025.1526718.
15. Purandare N, Ruiloba F, Nguyen-Hoang L, Wilailak S, Yanaihara N, Chung JP, et al. Cancer and fertility management: FIGO best practice advice. Int J Gynaecol Obstet. 2025;171(1):32-44. doi: 10.1002/ijgo.70426.
16. Matson J, Liu S. Fertility considerations young onset CRC. Semin Colon Rectal Surg. 2025;36(3):101119. doi: 10.1016/j.scrs.2025.101119.
17. Yu L, Berner J, Martinet A, Freund E, Singer D, von Woedtke T, et al. Gas plasma combination therapies-promises from preclinical oncology research. Antioxidants (Basel). 2025;14(9):1055. doi: 10.3390/antiox14091055.
18. Ammar MM, Ali R, Abd Elaziz NA, Habib H, Abbas FM, Yassin MT, et al. Nanotechnology in oncology: advances in biosynthesis, drug delivery, and theranostics. Discov Oncol. 2025;16(1):1172. doi: 10.1007/s12672-025-02664-3.
19. Weaver JMJ, Patey SJ. Systemic anti-cancer therapy and anaesthesia: a narrative review. Anaesthesia. 2025;80 Suppl 2:12-24. doi: 10.1111/anae.16522.
20. Allana A, Khowaja MA, Inayat A, Shamsi U, Rashid Y, Khan FR, et al. Assessing oral health-related quality of life in women undergoing chemotherapy for breast cancer in Karachi Pakistan. Sci Rep. 2025;15(1):7846. doi: 10.1038/s41598-025-91533-8.
21. Takei Y, Matsumoto A, Nomoto A, Kawashima M, Miyake Y, Kawakami A, et al. Early detection of drug-induced

interstitial lung disease using an electronic patient-reported outcome system: a report of two cases. Int Cancer Conf J. 2025. doi: 10.1007/s13691-025-00792-9.
22. Deng R, Lv J, Wang F, Chen Y, Wang J, Wang L, et al. Combination of epirubicin and cyclophosphamide for the treatment of advanced pulmonary sarcomatoid carcinoma: a case report and literature review. J Cancer Res Ther. 2025;21(2):512-7. doi: 10.4103/jcrt.jcrt_361_24.
23. Ghazizadeh S, Hosseini F, Malektojari A, Mahmoudi M, Azad A. Uterine inversion associated with uterine adenosarcoma in a 16-year-old: a case report with literature review. Indian J Gynecol Oncolog. 2025;23(1):36. doi: 10.1007/s40944-025-00968-4.
24. Assi S, Torrington E, Cheema E, Hamid AA. Adverse drug reactions associated with chemotherapeutic agents used in breast cancer: analysis of patients' online forums. J Oncol Pharm Pract. 2021;27(1):108-18. doi: 10.1177/1078155220915767.
25. Buchalska B, Kamińska K, Kowara M, Sobiborowicz-Sadowska A, Cudnoch-Jędrzejewska A. Doxorubicin or epirubicin versus liposomal doxorubicin therapy—differences in cardiotoxicity. Cardiovasc Toxicol. 2025;25(2):248-68. doi: 10.1007/s12012-024-09952-4.
26. Kouhen F, Afandi O, Benslima N, Bensalah O, Naciri M, Gouach HE, et al. A rare case of mediastinal liposarcoma: multidisciplinary approach and clinical challenges. Radiol Case Rep. 2025;20(9):4865-72. doi: 10.1016/j.radcr.2025.05.088.
27. Nedomansky J, Haslik W, Pluschnig U, Kornauth C, Deutschmann C, Hacker S, et al. Tissue distribution of epirubicin after severe extravasation in humans. Cancer Chemother Pharmacol. 2021;88(2):203-9. doi: 10.1007/s00280-021-04280-8.
28. Abolfazli P, Apue Nchama CN, Lucke-Wold B. Optimizing chemotherapy outcomes: the role of mindfulness in epirubicin treatment for urinary tumors. World J Psychiatry. 2025;15(4):102852. doi: 10.5498/wjp.v15.i4.102852.
29. Obispo B, Bailleux C, Cantos B, Zamora P, Jhawar SR, Varghese J, et al. Long-term adverse events following early breast cancer treatment with a focus on the BRCA-mutated population. Cancers (Basel). 2025;17(15):2506. doi: 10.3390/cancers17152506.
30. Treggiari E, Catania E, Valenti P, Boyd K, Finotello R. Factors associated with the development of gastrointestinal adverse events in dogs with multicentric lymphoma treated with CHOP or CEOP-based protocols: a multi-institutional, retrospective study. J Small Anim Pract. 2025;66(10):717-24. doi: 10.1111/jsap.13880.
31. Schaffrin-Nabe D, Josten-Nabe A, Heinze A, Tannapfel A, Schaffrin M, Voigtmann R. Optimizing scalp cooling: (ultra)structural follicular characteristic and restorative advances. Cancer Manag Res. 2025;17:1245-57. doi: 10.2147/cmar.S526775.
32. Deep A, Kumar D, Bansal N, Narasimhan B, Marwaha RK, Sharma PC. Understanding mechanistic aspects and therapeutic potential of natural substances as anticancer agents. Phytomed Plus. 2023;3(2):100418. doi: 10.1016/j.phyplu.2023.100418.
33. Mize BK, Salvi A, Ren Y, Burdette JE, Fuchs JR. Discovery and development of botanical natural products and their analogues as therapeutics for ovarian cancer. Nat Prod Rep. 2023;40(7):1250-70. doi: 10.1039/d2np00091a.
34. Liu H, Jin X, Liu S, Liu X, Pei X, Sun K, et al. Recent advances in self-targeting natural product-based nanomedicines. J Nanobiotechnology. 2025;23(1):31. doi: 10.1186/s12951-025-03092-9.
35. Nagy V, Mounir R, Szebeni GJ, Szakonyi Z, Gémes N, Minorics R, et al. Investigation of anticancer properties of monoterpene-aminopyrimidine hybrids on A2780 ovarian cancer cells. Int J Mol Sci. 2023;24(13):10581. doi: 10.3390/ijms241310581.
36. Ensoy M, Parıltı DN, Alkan AH, İlhan KN, Mutlu P, Dedeoğlu BG, et al. Evernic acid: a low-toxic and selective alternative to chemotherapeutic agents in the treatment of ovarian cancer. Arch Pharm (Weinheim). 2025;358(5):e70015. doi: 10.1002/ardp.70015.
37. Xu Z, Jiang Y, Shan T, Hu L, Wu M, Ji H, et al. Study on the effects and mechanism of corilagin on A2780 cell apoptosis. Curr Issues Mol Biol. 2025;47(2):105. doi: 10.3390/cimb47020105.
38. Villegas-Vazquez EY, Marín-Carrasco FP, Reyes-Hernández OD, Báez-González AS, Bustamante-Montes LP, Padilla-Benavides T, et al. Revolutionizing ovarian cancer therapy by drug repositioning for accelerated and cost-effective treatments. Front Oncol. 2024;14:1514120. doi: 10.3389/fonc.2024.1514120.
39. Das S, Biradar S, Jabin R, Datta S, Yasmin F, Babu RL, et al. In-silico inquest reveal the efficacy of *Usnea longissima* Ach. (A tropical lichen) against ovarian cancer. In Silico Pharmacol. 2025;13(2):116. doi: 10.1007/s40203-025-00408-3.
40. Kordylewski SK, Bugno R, Podlewska S. Residence time in drug discovery: current insights and future perspectives. Pharmacol Rep. 2025;77(4):851-73. doi: 10.1007/s43440-025-00748-z.
41. Abdelwahab AA, Elattar MA, Fawzi SA. Advancing ADMET prediction for major CYP450 isoforms: graph-based models, limitations, and future directions. Biomed Eng Online. 2025;24(1):93. doi: 10.1186/s12938-025-01412-6.
42. Kurniawan YS, Yudha E, Gurning K, Sholikhah EN, Pranowo HD, Jumina. Evaluation of xanthone-cinnamates as novel antibacterial agents against *Staphylococcus aureus* and *Escherichia coli*: in vitro and molecular docking insights. J Mol Struct. 2025;1345:143056. doi: 10.1016/j.molstruc.2025.143056.
43. Chen Z, Wang X, Huang W. Exploring the mechanism of Radix *Bupleuri* in the treatment of depression combined with SARS-CoV-2 infection through bioinformatics, network pharmacology, molecular docking, and molecular dynamic simulation. Metab Brain Dis. 2025;40(1):105. doi: 10.1007/s11011-025-01536-7.
44. Zhai M, Chen T, Shao M, Yang X, Qi Y, Kong S, et al. Unveiling the molecular mechanisms of Haitang-Xiaoyin Mixture in psoriasis treatment based on bioinformatics, network pharmacology, machine learning, and molecular docking verification. Comput Biol Chem. 2025;115:108352. doi: 10.1016/j.compbiolchem.2025.108352.
45. Oktriawan T, Ariefta N, Raharjo TJ, Astuti E, Koseki T, Shiono Y. Phytotoxic and cytotoxic polyketides produced by fungal endophytes isolated from *Psidium guajava*. HAYATI J Biosci. 2023;30(3):473-9. doi: 10.4308/hjb.30.3.473-479.

46. Areche C, Parra JR, Sepulveda B, García-Beltrán O, Simirgiotis MJ. UHPLC-MS metabolomic fingerprinting, antioxidant, and enzyme inhibition activities of *Himantormia lugubris* from Antarctica. Metabolites. 2022;12(6):560. doi: 10.3390/metabo12060560.
47. Ananto AD, Pranowo HD, Haryadi W, Prasetyo N. Flavonoid compound of red fruit Papua and its derivatives against SARS-CoV-2 Mpro: an in-silico approach. J Appl Pharm Sci. 2024;14(12):90-7. doi: 10.7324/japs.2024.177392.
48. Akter T, Rahman MM. Computational analysis of common gene and design protein-drug interaction network for the target diseases based on protein-protein interaction network in bioinformatics. Inform Med Unlocked. 2023;42:101357. doi: 10.1016/j.imu.2023.101357.
49. Basar MA, Hosen MF, Kumar Paul B, Hasan MR, Shamim SM, Bhuyian T. Identification of drug and protein-protein interaction network among stress and depression: a bioinformatics approach. Inform Med Unlocked. 2023;37:101174. doi: 10.1016/j.imu.2023.101174.
50. Haryadi W, Gurning K, Fachiroh J, Astuti E. Potential of bioactive compounds in *Coleus amboinicus* Lour., leaves against breast cancer by assessment using a network pharmacology approach and cytotoxic test. J Multidiscip Appl Nat Sci. 2025;5(1):267-87. doi: 10.47352/jmans.2774-3047.246.
51. Rehman AU, Khurshid B, Ali Y, Rasheed S, Wadood A, Ng HL, et al. Computational approaches for the design of modulators targeting protein-protein interactions. Expert Opin Drug Discov. 2023;18(3):315-33. doi: 10.1080/17460441.2023.2171396.
52. Olowosoke CB, Eze CJ, Munir A, Dada OO, Omolabake KE, Oke GA, et al. Integrative study of phytochemicals for anti-fibroid agent: a perspective on protein networks, molecular docking, ADMET, simulation, DFT and bioactivity. Chem Phys Impact. 2024;8:100412. doi: 10.1016/j.chphi.2023.100412.
53. Hossain MR, Tareq MM, Biswas P, Tauhida SJ, Bibi S, Zilani MN, et al. Identification of molecular targets and small drug candidates for Huntington's disease via bioinformatics and a network-based screening approach. J Cell Mol Med. 2024;28(16):e18588. doi: 10.1111/jcmm.18588.
54. Gurning K, Primahana G, Astuti E, Haryadi W. In vitro cytotoxic and molecular docking studies of the network pharmacology approach from bioactive compounds of *Coleus amboinicus* leaves against lung and breast cancer cells. Adv Pharmacol Pharm Sci. 2025;2025:5946648. doi: 10.1155/adpp/5946648.
55. Haryadi W, Gurning K, Astuti E. Molecular target identification of two *Coleus amboinicus* leaf isolates toward lung cancer using a bioinformatic approach and molecular docking-based assessment. J Appl Pharm Sci. 2024;14(5):203-10. doi: 10.7324/japs.2024.164753.
56. Yang C, Xin Y, Wang G, Ma H, Jing L. Protective mechanism of moslosooflavone against hypobaric hypoxia-induced brain injury: insights from network pharmacology and in vivo validation. Eur J Pharmacol. 2025;1004:178001. doi: 10.1016/j.ejphar.2025.178001.
57. Kurniawan YS, Yudha E, Nugraha G, Fatmasari N, Pranowo HD, Jumina J, et al. Molecular docking and molecular dynamic investigations of xanthone-chalcone derivatives against epidermal growth factor receptor for preliminary discovery of novel anticancer agent. Indones J Chem. 2024;24(1):250-66. doi: 10.22146/ijc.88449.
58. Alom MM, Faruqe MO, Molla MK, Rahman MM. Exploring prognostic biomarkers of acute myeloid leukemia to determine its most effective drugs from the FDA-approved list through molecular docking and dynamic simulation. Biomed Res Int. 2023;2023:1946703. doi: 10.1155/2023/1946703.
59. Gholami A, Minai-Tehrani D, Mahdizadeh SJ, Saenz-Mendez P, Eriksson LA. Structural insights into *Pseudomonas aeruginosa* exotoxin a-elongation factor 2 interactions: a molecular dynamics study. J Chem Inf Model. 2023;63(5):1578-91. doi: 10.1021/acs.jcim.3c00064.
60. An X, Zhang W, Rong C, Liu S. Understanding Ramachandran plot for dipeptide: a density functional theory and information-theoretic approach study. J Chin Chem Soc. 2023;70(3):243-52. doi: 10.1002/jccs.202200444.
61. Nikakhtar S, Nafari A, Barzegari A, Parvarinezhad S, Eshaghi Malekshah R, Gholivand K. Novel phosphoramide ligand shows promise as a cytotoxic agent against breast cancer: molecular docking, ADMET studies and quantum studies. Results Chem. 2025;16:102520. doi: 10.1016/j.rechem.2025.102520.
62. Poh AR, Ernst M. Functional roles of SRC signaling in pancreatic cancer: recent insights provide novel therapeutic opportunities. Oncogene. 2023;42(22):1786-801. doi: 10.1038/s41388-023-02701-x.
63. Feng Z, Wei W, Wang S, Li X, Zhao L, Wan G, et al. A novel selective FAK inhibitor E2 inhibits ovarian cancer metastasis and growth by inducing cytotoxic autophagy. Biochem Pharmacol. 2024;229:116461. doi: 10.1016/j.bcp.2024.116461.
64. Attia SM, Ahmad SF, Okash RM, Bakheet SA. Aneugenic effects of epirubicin in somatic and germinal cells of male mice. PLoS One. 2014;9(10):e109942. doi: 10.1371/journal.pone.0109942.